Contents lists available at ScienceDirect

Applied Catalysis B: Environmental

Highly efficient and stable hydrogen evolution from water with CdS as photosensitizer—A noble-metal-free system

Jian-Ping Zou [a,*], Si-Liang Lei [a], Jian Yu [a], Sheng-Lian Luo [a,*], Xu-Biao Luo [a], Xing-Hua Tang [a], Wei-Li Dai [a], Jing Sun [b], Guo-Cong Guo [b], Chak-Tong Au [a,c]

[a] Key Laboratory of Jiangxi Province for Persistent Pollutants Control and Resources Recycle, Nanchang Hangkong University, Nanchang 330063, Jiangxi, PR China
[b] State Key Laboratory of Structural Chemistry, Fujian Institute of Research on the Structure of Matter, Chinese Academy of Sciences, Fuzhou 350002, Fujian, PR China
[c] Department of Chemistry, Hong Kong Baptist University, Kowloon Tong, Hong Kong, PR China

ABSTRACT

$CdS/Ba_{1-x}Zn_xTiO_3$ heterostructured photocatalysts were developed as a highly efficient and stable system for photocatalytic evolution of hydrogen from water splitting. In the system, CdS not only functions as photosensitizer to absorb visible light, but also participates with $Ba_{1-x}Zn_xTiO_3$ for the generation of heterojunctions that block the recombination of photogenerated electrons and holes. The photocatalysts show excellent activity and stability, giving a high H_2 production rate of $1473\,\mu mol\,h^{-1}\,g^{-1}$ under the irradiation of simulated solar light in a test period of 480 h without loading any noble metal as cocatalyst or any reagents for regeneration. This study demonstrates that the development of CdS nanoparticles as photosensitizer is feasible for the photocatalytic H_2 production.

© 2014 Elsevier B.V. All rights reserved.

1. Introduction

Since the discovery of Fujishima and Honda on the photocatalytic splitting of water over TiO_2 electrodes [1–3], there are numerous reports on the synthesis and use of photocatalysts for water splitting, but most of them are active only under UV irradiation [4]. With respect to solar energy, only a small fraction (ca. 4%) lies in the ultraviolet region, whereas the visible light in the solar spectrum is far more abundant (ca. 46%) [5]. For better efficiency of capturing solar energy, it is desirable to develop visible-light-driven photocatalysts. One of the adopted strategies is to modify a photocatalyst of wide band gap with a photosensitizer [6], and the common photosensitizers are organic dyes [7,8]. Nonetheless, these light-absorbing molecules decompose under working conditions within hours [6]. Hence, the development of stable photosensitizers is a key issue. In the past four decades, photosensitizers based on noble metals such as $[Ru(bipy)_3]^{2+}$ were successfully used in photocatalytic hydrogen evolution [9,10,8]. However, noble metals are rare and expensive, and the mining of

them is harmful to the environment [11]. It is hence desirable to develop catalytic systems that are free from noble metals.

Compared to the use of traditional organic or organometallic light-absorbing molecules, it is more economical to use semiconductor nanocrystals as photosensitizers. It is known that the semiconductor nanocrystals are photostable, and can deliver multiple electrons with minimal structural perturbation [12,13]. Recently, the nanocrystals of chalcogenides were employed as photosensitizers in photocatalytic systems [14,15], but their use for the evolution of hydrogen from water is rare [16–18]. Furthermore, the photocatalytic properties, especially long-term durability, are still needed to improve when chalcogenides are used as photosensitizers of catalysts for H_2 production due to high recombination rate of photogenerated electrons and holes and limited photostability [19–22].

We are interested in developing a noble-metal-free system that is efficient for the photocatalytic generation of hydrogen from water. It is known that the band gap of CdS nanocrystals is small and the conduction band (CB) of CdS is suitable for hydrogen production [23,24]. More importantly, CdS possesses a band structure that matches that of $Ba_{1-x}Zn_xTiO_3$ solid solution. We envisage that coupling CdS with $Ba_{1-x}Zn_xTiO_3$ would result in a high-efficient photocatalyst with good durability for H_2 evolution from water splitting. It is because CdS can act as photosensitizer for

* Corresponding author. Tel.: +86 791 83863688/+86 791 83863373;
fax: +86 791 83953373.
E-mail addresses: zjp_112@126.com (J.-P. Zou), sllou@hnu.edu.cn (S.-L. Luo).

light-harvesting and a combination of CdS with $Ba_{1-x}Zn_xTiO_3$ would result in the formation of heterojunctions that hinder the recombination of photogenerated holes and electrons. The present work demonstrates that CdS nanocrystals photosensitizing $Ba_{1-x}Zn_xTiO_3$ is an economic and effective approach to obtain a noble-metal-free system with excellent photocatalytic activity and long-term durability for H_2 generation from water.

2. Experimental

2.1. Materials and measurement

All chemicals were analytically pure and used without further purification. The crystalline phases of samples were investigated by X-ray diffraction (Bruker D8 ADVANCE) using graphite monochromatized Cu $K\alpha$ ($\lambda = 1.5406$ Å) radiation. The XRD data for indexing and cell-parameter calculations were collected in a scan mode with a scanning speed of $2°$/min in the 2θ range between $10°$ and $70°$. The morphology of samples was studied with a scanning electron microscope (SEM, FEI, Holand) and a transmission electron microscope (TEM). Composition analyses on several randomly selected samples of the as-prepared catalysts were performed on a field-emission scanning electron microscope equipped with an energy dispersive X-ray spectroscope (EDS). X-ray photoelectron spectroscopy (XPS) measurements were taken with a VG Escalab 250 spectrometer equipped with an Al anode (Al $K\alpha = 1486.7$ eV). UV–vis diffuse reflectance spectra were measured with a PE Lambda 900 UV/Vis spectrophotometer at room temperature. Photoluminescence recording was performed on a fluorescence spectrometer (F-7000, Hitachi, Japan).

Electrochemical measurements were performed on a CHI 660D electrochemical workstation (Shanghai Chenhua, China) using a standard three-electrode cell with a working electrode, a graphite electrode as counter electrode, and a standard calomel electrode in saturated KCl as reference electrode. The working electrodes were prepared by dip-coating: 20 mg of photocatalyst was suspended in 5 mL ethanol to produce slurry that was then dip-coated onto a 2 cm × 0.5 cm fluorine-tin oxide (FTO) glass electrode. After drying under ambient condition, the films were sintered at $300°$C for 1 h. The electrolyte (Na_2S/Na_2SO_3: Na_2S 0.35 M, Na_2SO_3 0.25 M) was purged with nitrogen. As for photocurrent measurements, a 300 W xenon lamp was used to generate simulated sunlight and the other conditions were similar to those of electrochemical measurements.

2.2. Syntheses

2.2.1. Syntheses of $Ba_{1-x}Zn_xTiO_3$ solid solutions

The $Ba_{1-x}Zn_xTiO_3$ ($x = 0$, 0.05, 0.1, 0.15, and 0.2) solid solutions were synthesized by a hydrothermal-gel method. In a typical procedure, solution A was prepared by dissolving stoichiometric amounts of barium acetate (0.01–0.01x mol) and zinc acetate (0.01x mol) in 10 mL 36% acetic acid solution. Solution B was prepared by dissolving 3.4 mL of tetrabutyltitanate (0.01 mol) in 5 mL isopropanol and then 1.5 mL of acetic acid was added. Solution B was slowly added to solution A and the resulted mixture was magnetically stirred for 30 min. Then the mixture was hydrothermally treated in a 25 mL Teflon-lined stainless steel autoclave at $100°$C for 2 h. The resulting gel was calcined at $900°$C for 10 h. The as-synthesized products with $x = 0$, 0.05, 0.1, 0.15, and 0.2 are designated as $BaTiO_3$, $Ba_{0.95}Zn_{0.05}TiO_3$, $Ba_{0.9}Zn_{0.1}TiO_3$, $Ba_{0.85}Zn_{0.15}TiO_3$, and $Ba_{0.8}Zn_{0.2}TiO_3$, respectively.

2.2.2. Syntheses of heterostructured $CdS/Ba_{1-x}Zn_xTiO_3$

The heterostructured composites $CdS/Ba_{1-x}Zn_xTiO_3$ ($x = 0$, 0.05, 0.1, 0.15, and 0.2) with different CdS loadings (based on initial molar ratio of Cd/Ti) were synthesized by solvothermal method.

Typically, the as-synthesized $Ba_{1-x}Zn_xTiO_3$ solid solution was dispersed in 30 mL deionized water under magnetic stirring. Then under ultrasonic treatment, stoichiometric cadmium acetate solution and thiourea solution was added in a span of 15 min. Finally, the mixture was hydrothermally treated in a 100 mL Teflon-lined stainless steel autoclave at $150°$C for 10 h. The resulting samples were separated by filtration, washed several times with deionized water and alcohol and then dried at $90°$C for 12 h. Hereinafter, the heterostructured $CdS/Ba_{0.9}Zn_{0.1}TiO_3$ containing 10%, 20%, 30% and 40% (atom%) CdS are denoted hereinafter as 10CBZTO, 20CBZTO, 30CBZTO and 40CBZTO, respectively.

2.3. Photocatalytic activity for water splitting

Photocatalytic reactions were carried in a Pyrex top-irradiation reaction vessel with a capacity of 100 mL connected to a glass closed gas system (PerfectLight). A 300 W Xe lamp (PerfectLight, wavelength Range: 320 nm $\leq \lambda \leq$ 780 nm, light intensity: 160 mW cm^{-2}) was used to generate simulated sunlight and visible light (cutoff filter applied for the latter, $\lambda > 420$ nm). H_2 production was performed by dispersing 25 mg of catalyst in an aqueous solution (80 mL) containing Na_2S/Na_2SO_3 (Na_2S 0.35 M, Na_2SO_3 0.25 M) as sacrificial reagents. The reaction solution was evacuated several times to remove air completely prior to irradiation. The temperature of the reaction solution was maintained at $6°$C by a continuous flow of cold water (constant temperature device XODC-0506, Nanjing Shunliu, China) during the reaction. The evolved gases were in situ analyzed by gas chromatography equipped with a thermal conductive detector (TCD) and a 5 Å molecular sieve column, using argon as the carrier gas.

3. Results and discussion

3.1. Characterization of materials

The XRD patterns of $Ba_{1-x}Zn_xTiO_3$ ($x = 0$, 0.1 and 0.2) are shown in Fig. 1a. It is clear that the patterns of $Ba_{1-x}Zn_xTiO_3$ ($x = 0$, 0.1, and 0.2) are similar to that of cubic $BaTiO_3$ (JCPDS No. 01-075-0461). The doping of Zn^{2+} does not obviously change the crystalline structure of $BaTiO_3$. A careful comparison of the (1 1 0) diffraction peaks in the 2θ range of $31–32.5°$ (the inset of Fig. 1a) shows that with the increase of Zn^{2+} doping, the XRD peak positions shift to slightly higher angles. The result indicates that there is partial substitution of Ba^{2+} by Zn^{2+} because the ionic radius of Zn^{2+} (0.074 nm) is smaller than that of Ba^{2+} (0.135 nm) but larger than that of Ti^{4+} (0.0605 nm). Based on similar results of XRD analysis reported in the literature [2,25,26], one can accept that our $Ba_{1-x}Zn_xTiO_3$ are solid solutions rather than mixtures of $BaTiO_3$ and $ZnTiO_3$.

Fig. 1b shows the XRD patterns of $CdS/Ba_{0.9}Zn_{0.1}TiO_3$ loaded with different amounts of CdS (10CBZTO, 20CBZTO, 30CBZTO and 40CBZTO). The diffraction profiles indicate a mixture of $Ba_{0.9}Zn_{0.1}TiO_3$ and hexagonal CdS (JCPDS No. 00-002-0549), and there is no detection of impurity phase. As the amount of CdS increases from 10% to 40%, the peaks of hexagonal CdS intensify and there is no change of position of the major $Ba_{0.9}Zn_{0.1}TiO_3$ peaks. The results indicate that the loading of CdS does not change of $Ba_{0.9}Zn_{0.1}TiO_3$ crystal structure.

The UV–vis absorption spectra of $BaTiO_3$, $Ba_{0.9}Zn_{0.1}TiO_3$, CdS, 10CBZTO, 20CBZTO, 30CBZTO and 40CBZTO are shown in Fig. 2. Compared to $BaTiO_3$, $Ba_{0.9}Zn_{0.1}TiO_3$ exhibits an absorption edge that is slightly red-shifted, but light absorption is still in the UV region with a band edge of approximately 3.1 eV. After CdS sensitization, there is clear absorption of visible light. And with increase of CdS loading (from 10% to 40%), there is continuous red shift of
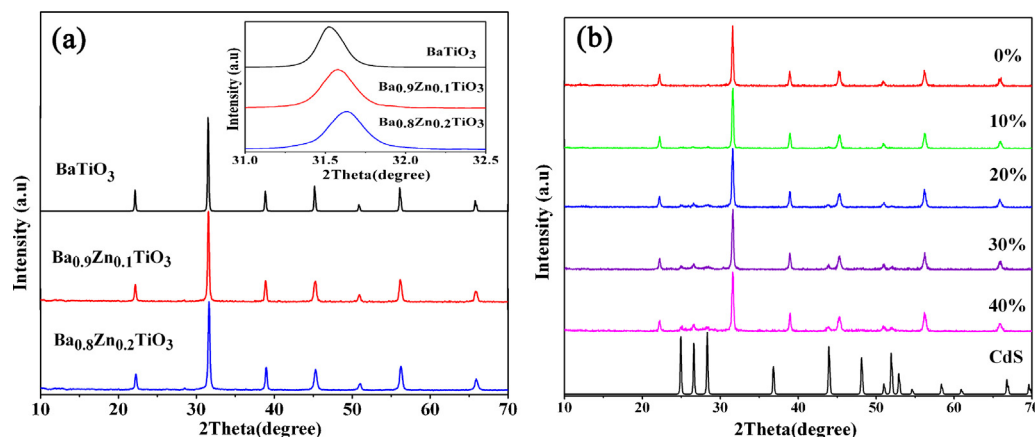
Fig. 1. XRD patterns of (a) $Ba_{1-x}Zn_xTiO_3$ ($x = 0, 0.1$ and 0.2) solid solutions and (b) $Ba_{0.9}Zn_{0.1}TiO_3$ loaded with different amounts of CdS.

absorption edges. The results indicate that with CdS as photosensitizer for $Ba_{0.9}Zn_{0.1}TiO_3$, there is better harvest of solar light.

The morphology and microstructure of the as-prepared samples were revealed by SEM and TEM. Fig. 3a–d shows the SEM images of 10CBZTO, 20CBZTO, 30CBZTO and 40CBZTO. It is observed that the as-synthesized $CdS/Ba_{1-x}Zn_xTiO_3$ catalysts are all in form of heterostructured nanocomposites, showing uniform distribution of CdS nanoparticles ($\sim$25 nm in size) on the surface of $Ba_{0.9}Zn_{0.1}TiO_3$. With the increase of CdS loading, there is higher amount of CdS nanoparticles on the surface of $Ba_{0.9}Zn_{0.1}TiO_3$. Furthermore, there are certain degree of CdS aggregation in 30CBZTO, and 40CBZTO. The TEM image of 20CBZTO (Fig. 3e) also reveals that there is homogeneous dispersion of CdS nanoparticles on $Ba_{0.9}Zn_{0.1}TiO_3$. The HRTEM image of 20CBZTO (Fig. 3f) clearly shows the interface of CdS and $Ba_{0.9}Zn_{0.1}TiO_3$, as well as the high crystallinity of the heterostructured nanocomposite. The fringes of $d = 0.390$ nm and $d = 0.314$ nm are in agreement with the (0 1 0) planes of $Ba_{0.9}Zn_{0.1}TiO_3$ and the (1 0 1) planes of CdS, respectively. It well demonstrates that there is the formation of heterojunctions at the $Ba_{0.9}Zn_{0.1}TiO_3$ and CdS interfaces.

The chemical states of $Ba_{0.9}Zn_{0.1}TiO_3$ and 20CBZTO were studied by XPS. Fig. S1a and b shows the $Ba-3d_{3/2}$ and $Ba-3d_{5/2}$ peaks of $Ba_{0.9}Zn_{0.1}TiO_3$ at 794.60 and 779.35 eV (binding energy) and the $Zn-2p_{1/2}$ and $Zn-2p_{3/2}$ peaks of $Ba_{0.9}Zn_{0.1}TiO_3$ at 1045.43 and 1021.71 eV, respectively. The results show that the

Ba and Zn species in $Ba_{0.9}Zn_{0.1}TiO_3$ are both divalent. The $Ti-2p_{1/2}$ and $Ti-2p_{3/2}$ binding energies of $Ba_{0.9}Zn_{0.1}TiO_3$ are 464.17 and 458.45 eV (Fig. S1c), respectively, indicating that the Ti species in $Ba_{0.9}Zn_{0.1}TiO_3$ are tetravalent. As shown in Fig. S1d, the O-1s peak is located at 530.40 eV, which can be assigned to oxygen (Ti–O) of crystal lattice. Nonetheless, these values are slightly different from those of $BaTiO_3$ or $ZnTiO_3$ reported by Reddy et al. [27,28], indicating that the local chemical environment of the elements in $Ba_{0.9}Zn_{0.1}TiO_3$ is different from that of $BaTiO_3$. Combined with the XRD results of $Ba_{1-x}Zn_xTiO_3$, it is deduced that there is successful synthesis of $Ba_{1-x}Zn_xTiO_3$ solid solutions. With the loading of CdS, there is a slight change in peak positions with respect to those of $Ba_{0.9}Zn_{0.1}TiO_3$ (Fig. S1a–d), suggesting that the introduction of CdS causes a change of chemical environment of the elements. Furthermore, XPS signals of Cd-3d (Fig. S1e) and S-2p (Fig. S1f) are observed at binding energies of around 411.99 eV ($Cd-3d_{3/2}$), 405.20 eV ($Cd-3d_{5/2}$) and 161.48 eV (S-3p), respectively, which are consistent with those of CdS reported by Yu et al. [29]. The results indicate that there is successful synthesis of the heterostructured 20CBZTO composite.

3.2. Photocatalytic results

As shown in Fig. 4, the $Ba_{1-x}Zn_xTiO_3$ ($x = 0.05, 0.1, 0.15$, and 0.2) solid solutions have certain levels of photoactivity under simulated solar irradiation for water splitting, and $Ba_{0.9}Zn_{0.1}TiO_3$ is the highest in performance, showing a H_2 evolution rate of about 364 μmol h^{-1} g^{-1}. It is well known that because the bottom of the conduction band (CB) of $BaTiO_3$ is more positive than the reduction potential of H^+/H_2, $BaTiO_3$ cannot function as photocatalyst for H_2 evolution from water splitting. We found that with partial substitution of Ba^{2+} with Zn^{2+}, the resulted $Ba_{1-x}Zn_xTiO_3$ is a kind of photocatalysts active for H_2 evolution from water splitting. The results demonstrate that forming solid solutions is a promising method to obtain catalysts with good photocatalytic activity.

We evaluated the photocatalytic activity of 10CBZTO, 20CBZTO, 30CBZTO and 40CBZTO for H_2 production from water splitting under the irradiation of simulated sunlight. As show in Fig. 5a, when $Ba_{0.9}Sr_{0.1}TiO_3$ was sensitized with CdS, there is significant improvement of H_2 production. The maximum H_2 production rate is observed over 20CBZTO (1473 μmol h^{-1} g^{-1}), which is higher than those of most semiconductor photocatalysts, and even higher than those of some semiconductor photocatalysts loaded with noble metals as reported in the literature (Table S1 in SI). The results indicate that the use of CdS nanoparticles as photosensitizer is effective. For comparison, we also investigated the photocatalytic activity of CdS as well as that of mechanically mixed CdS and $Ba_{0.9}Zn_{0.1}TiO_3$ under the same conditions. As show in Fig. 5a,
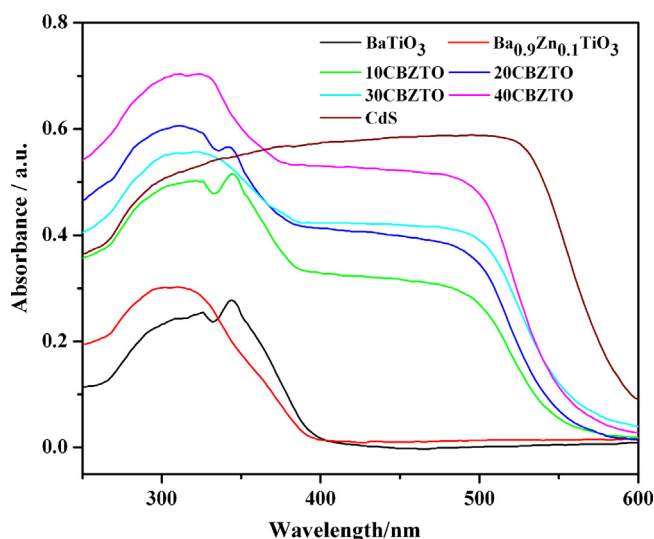

Fig. 2. UV–vis absorbance spectra of as-prepared photocatalysts.
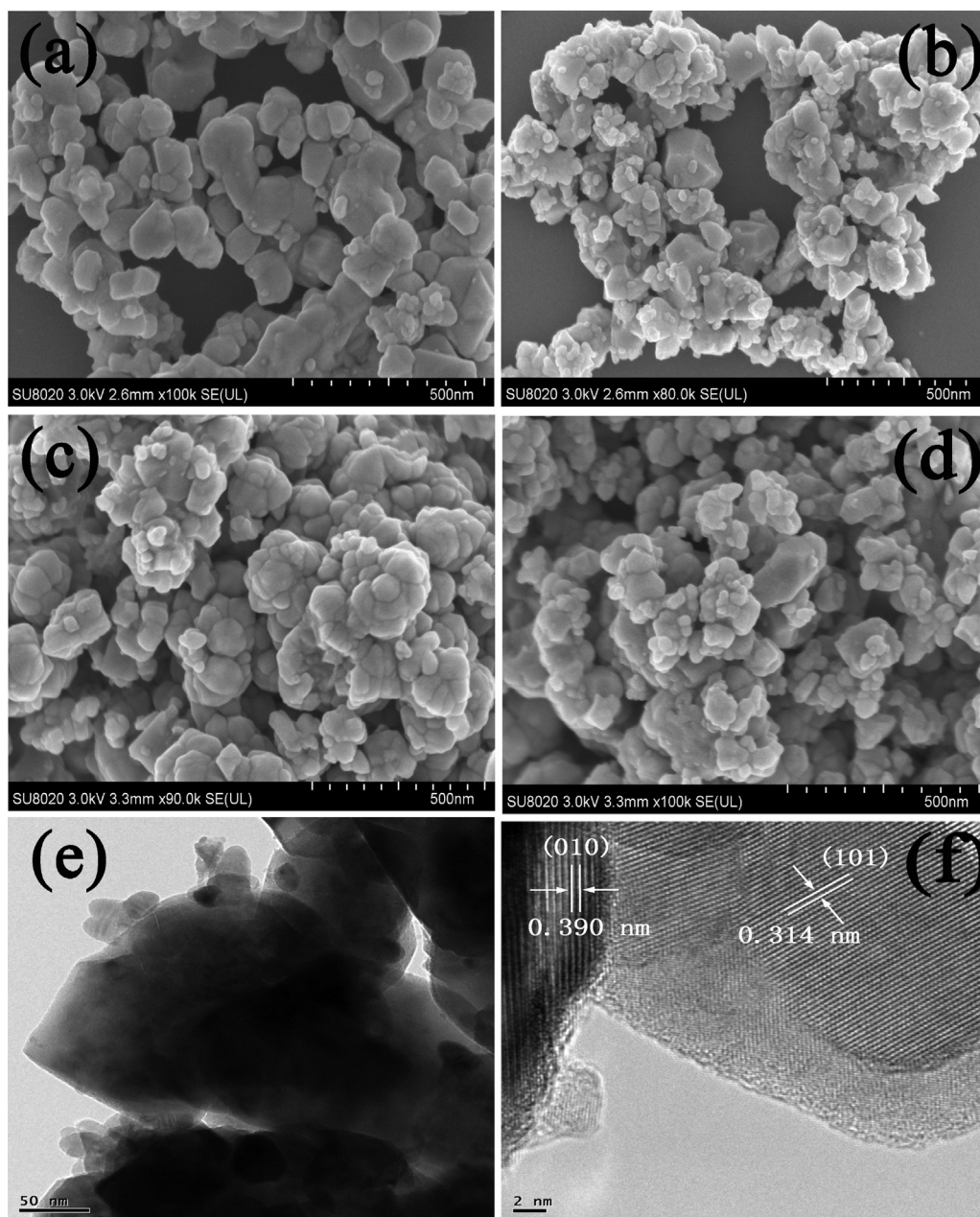
Fig. 3. SEM images of (a) 10CBZTO, (b) 20CBZTO, (c) 30CBZTO and (d) 40CBZTO as well as (e) TEM image and (f) HRTEM image of 20CBZTO.

the CdS and the mechanically mixed samples show photocatalytic activity much worse than that of 20CBZTO. The results indicate that simple mechanical mixing is not able to create effective interfacial contacts between CdS and $Ba_{0.9}Zn_{0.1}TiO_3$ solid solution, which is crucial for the electron transfer between them. In other words, there is the creation of heterojunctions at the interfaces of CdS and $Ba_{0.9}Zn_{0.1}TiO_3$ in the CdS/$Ba_{0.9}Zn_{0.1}TiO_3$ composites. In addition, we studied the photocatalytic activity of 20%CdS/$Ba_{1-x}Zn_xTiO_3$ ($x = 0.05$, 0.1, 0.15, and 0.2) under the same conditions (Fig. S2). The results show that the heterostructured 20CBZTO has the best photocatalytic activity among them.

Fig. 5b shows the photocatalytic activity over CdS/$Ba_{0.9}Zn_{0.1}TiO_3$ for water splitting under the irradiation of visible light. Using $Ba_{0.9}Zn_{0.1}TiO_3$ alone does not result in hydrogen production in the visible-light region because of the band gap of $Ba_{0.9}Zn_{0.1}TiO_3$ is wide. With the loading of CdS, there is great improvement of photocatalytic activity. Under visible-light irradiation, the rate of

hydrogen evolution over 20CBZTO is 561 $\mu mol\,h^{-1}\,g^{-1}$, which is the best among the prepared CdS/$Ba_{0.9}Zn_{0.1}TiO_3$ catalysts, a trend similar to that when simulated solar light is used as irradiation source. The results demonstrate that CdS is a good photosensitizer for the design of high-performance photocatalysts.

Fig. 6a shows the evolution of hydrogen over 20CBZTO under simulated solar irradiation for thirty consecutive runs. There is steady evolution of hydrogen across the thirty runs and the rate of hydrogen evolution remains around 1473 $\mu mol\,h^{-1}\,g^{-1}$. Although there is a slight decline of rate after 100 h, the rate recovers upon replenishment of sacrificial reagents, and the same phenomenon was repeated after 260 h. Thus the little decrease of photoactivity is due to consumption of sacrificial reagents rather than deactivation of photocatalyst. Plotted in Fig. 6b is the evolution of H_2 as a function of time. One can see that the rate of hydrogen evolution is steady within the 480-h run. In addition, the XRD and TEM results of the 20CBZTO sample collected after 480 h of
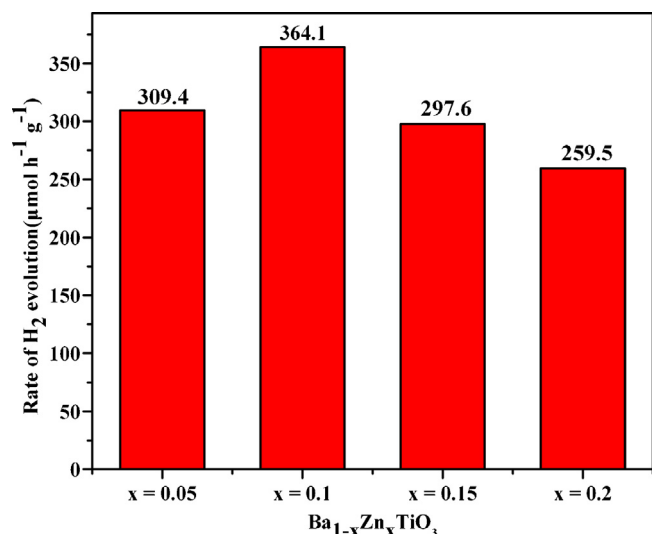
Fig. 4. The rate of hydrogen evolution over $Ba_{1-x}Zn_xTiO_3$ ($x = 0.05, 0.1, 0.15$ and 0.2) under simulated solar irradiation using Na_2S/Na_2SO_3 (Na_2S 0.35 M, Na_2SO_3 0.25 M) as sacrificial reagent.

photocatalytic reaction are similar to those of the fresh sample (Figs. S3 and S4a). Although the HRTEM image (Fig. S4b) of the recovered sample is not exactly the same as that of the fresh sample, the lattice fringes of CdS (1 0 1) and $Ba_{0.9}Zn_{0.1}TiO_3$ (0 1 0) can still be seen. All of these indicate that 20CBZTO is stable and durable for the

photocatalytic reaction. Compared with the catalysts using semiconductor nanocrystals or organic and organometallic molecules as photosensitizers [10,30,31], the catalyst resulted from the use of CdS as photosensitizer is superior in terms of efficiency, stability and durability. To the best of our knowledge, this is the first example of a photocatalyst that exhibits excellent activity and durability for H_2 production from water splitting without the use of a noble metal as cocatalyst or a reagent for regeneration [32,33].

3.3. Mechanism of photocatalytic activity enhancement

The photocurrent responses of the prepared samples were investigated for several on-off cycles under simulated solar irradiation. As shown in Fig. S5, fast photocurrent responses are observed over both electrodes and the phenomenon is reversible, exhibiting good reproducibility. The obvious enhancement of photocurrent observed over $CdS/Ba_{0.9}Zn_{0.1}TiO_3$ indicates that the separation efficiency of photo-induced electrons and holes is improved due to the heterojunctions at the CdS and $Ba_{0.4}Sr_{0.6}TiO_3$ interfaces. The photocurrent response of 20CBZTO is the highest and the phenomenon can be related to the best photocatalytic activity of 20CBZTO as compared with that of $Ba_{0.9}Zn_{0.1}TiO_3$ or those of $Ba_{0.9}Zn_{0.1}TiO_3$ loaded with different amounts of CdS. Furthermore, the better separation of photogenerated electrons and holes in $CdS/Ba_{0.9}Zn_{0.1}TiO_3$ was also confirmed by the PL spectra of $Ba_{0.9}Zn_{0.1}TiO_3$ and 20CBZTO. As shown in Fig. S6, 20CBZTO exhibits much lower emission intensity than $Ba_{0.9}Zn_{0.1}TiO_3$, indicating that the recombination of photogenerated charge carriers was greatly inhibited in $CdS/Ba_{0.9}Zn_{0.1}TiO_3$ due to the created heterojunctions.
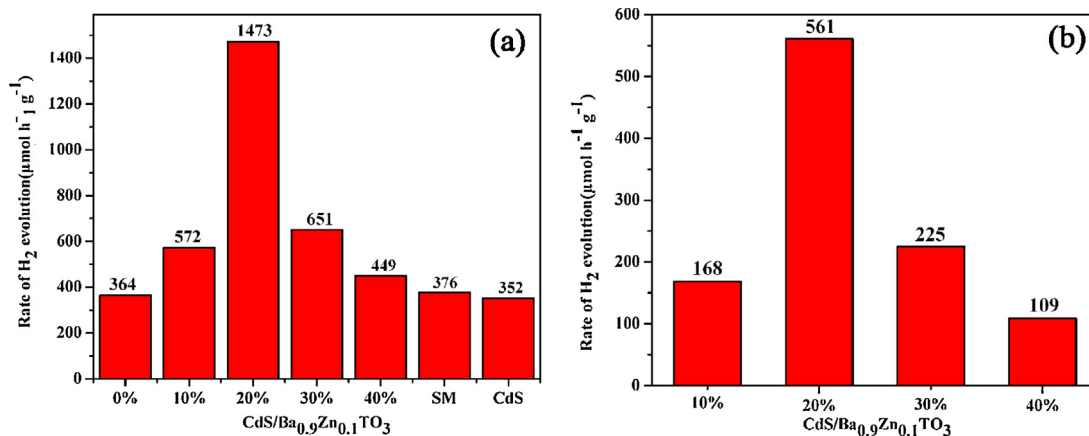

Fig. 5. The rate of hydrogen evolution over $CdS/Ba_{0.9}Zn_{0.1}TiO_3$ with different amounts of CdS under the irradiation of (a) simulated sunlight and (b) visible light using Na_2S/Na_2SO_3 (Na_2S 0.35 M, Na_2SO_3 0.25 M) as sacrificial reagent (SM represents the sample of physically mixed $Ba_{0.9}Zn_{0.1}TiO_3$ and CdS).
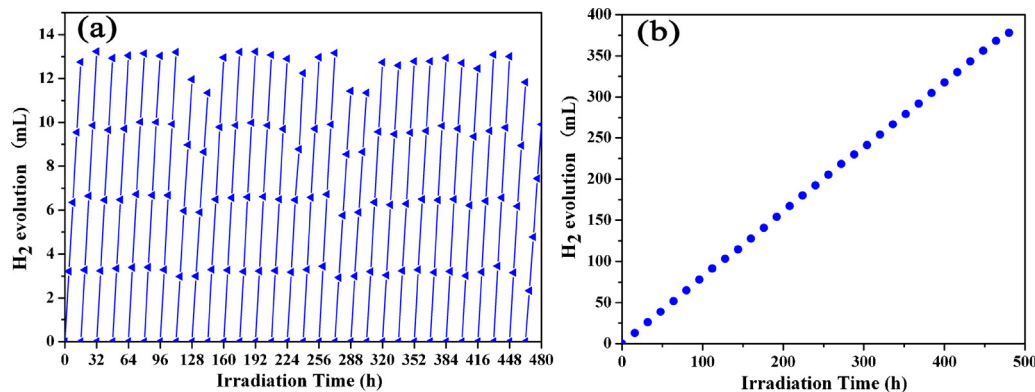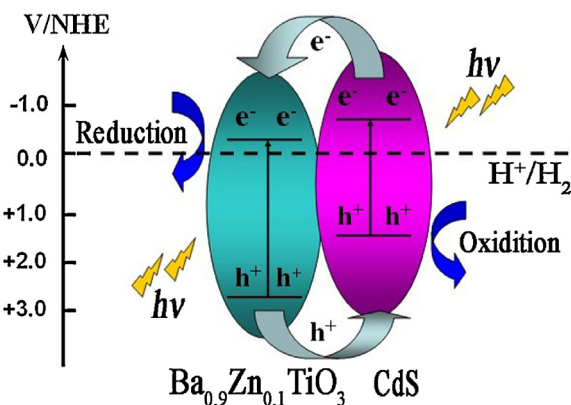

Fig. 6. (a) Hydrogen evolution using 20CBZTO under simulated solar irradiation for thirty consecutive runs (Na_2S/Na_2SO_3 as sacrificial reagents) and (b) Total H_2 evolution using 20CBZTO in 480 h under simulated solar irradiation (Na_2S/Na_2SO_3 as sacrificial reagents).

Scheme 1. Energy band diagram and photocatalytic scheme of the CdS/Ba$_{0.9}$Zn$_{0.1}$TiO$_3$ heterostructured system.

The electrochemical properties of the photocatalysts were studied using a standard three-electrode cell. Fig. S7 shows the Mott–Sckottky (MS) plots with Ba$_{0.9}$Zn$_{0.1}$TiO$_3$ and CdS being working electrodes (0.5 M K$_2$SO$_4$ with pH of 7 as electrolyte). The values of V_{fb} are calculated to be -0.30 and -0.65 eV vs. SCE (equivalent to -0.06 and -0.41 eV vs. NHE, respectively) for Ba$_{0.9}$Zn$_{0.1}$TiO$_3$ and CdS, respectively. Based on these data, the CB of Ba$_{0.9}$Zn$_{0.1}$TiO$_3$ and CdS are calculated to be -0.26 and -0.51 eV, whereas the VB of Ba$_{0.9}$Zn$_{0.1}$TiO$_3$ and CdS are calculated as 2.84 and 1.49 eV, respectively.

According to the above results, Scheme 1 is proposed to illustrate the energy band levels of CdS/Ba$_{0.9}$Zn$_{0.1}$TiO$_3$ as well as the possible charge-separation processes. Under simulated solar irradiation, both CdS and Ba$_{0.9}$Zn$_{0.1}$TiO$_3$ are easily excited and there is the generation of photogenerated electrons and holes. Since the potentials of CB and VB of CdS are more negative than those of Ba$_{0.9}$Zn$_{0.1}$TiO$_3$, the photogenerated electrons (e$^-$) in the CB of CdS flow to the CB of Ba$_{0.9}$Zn$_{0.1}$TiO$_3$, whereas the holes (h$^+$) formed in the VB of Ba$_{0.9}$Zn$_{0.1}$TiO$_3$ migrate to the VB of CdS. Thus, CdS nanocrystals can be regarded as photosensitizer because they absorb visible light and generate photoelectrons that transfer to the CB of Ba$_{0.9}$Zn$_{0.1}$TiO$_3$. With effective charge separation, the separated electrons have long enough time to reduce H$^+$ to H$_2$ on the surfaces of Ba$_{0.9}$Zn$_{0.1}$TiO$_3$, while the holes oxidize the Na$_2$S/Na$_2$SO$_3$ sacrificial reagents. In addition, under visible-light irradiation, only CdS can be excited to produce photoelectrons and holes, and the electrons in the CB of CdS flow into the CB of Ba$_{0.9}$Zn$_{0.1}$TiO$_3$, while the same amount of holes are left in the VB of CdS. This scenario favors the separation of photogenerated electrons and holes, and consequently results in enhancement of photocatalytic activity. Since the amount of electrons and holes generated under visible light is smaller than those produced under solar light irradiation, the photocatalytic efficiency over 20CBZTO under visible-light is inferior to that under solarlight, in consistent with the photocatalytic results. The mechanism demonstrates that CdS acts as photosensitizer for the absorption of visible light as well as combines with Ba$_{0.9}$Zn$_{0.1}$TiO$_3$ for the formation of heterojunctions.

4. Conclusions

A new kind of heterostructured CdS/Ba$_{1-x}$Zn$_x$TiO$_3$ nanocomposites with CdS nanocrystals as photosensitizer was developed and used as photocatalysts for H$_2$ evolution from water splitting. The 20CBZTO photocatalyst exhibits the best activity, showing a H$_2$ production rate of 1473 μmol h^{-1} g^{-1} and remaining stable and durable under the irradiation of simulated solar light in a test period of 480 h without loading noble metals as cocatalysts and reagents for regeneration. The excellent performance is attributed to the effective absorption of light energy by CdS photosensitizer as well as to the creation of heterojunctions at the CdS and Ba$_{1-x}$Zn$_x$TiO$_3$ interfaces for effective separation of photogenerated electrons and holes. The study of the CdS/Ba$_{1-x}$Zn$_x$TiO$_3$ system opens up a new avenue for the preparation of low-cost and high-performance photocatalysts that are efficient, stable and durable for hydrogen evolution from splitting of water.

Appendix A. Supplementary data

Supplementary material related to this article can be found, in the online version, at http://dx.doi.org/10.1016/j.apcatb. 2013.12.047.

References

[1] A. Fujishima, K. Honda, Nature 238 (1972) 37.
[2] S.S. Chen, J.X. Yang, C.M. Ding, R.G. Li, S.Q. Jin, D.E. Wang, H.X. Han, F.X. Zhang, C. Li, J. Mater. Chem. A 1 (2013) 5651.
[3] Y.B. Wu, P. Lazic, G. Hautier, K. Perssonb, G. CedeR, Energy Environ. Sci. 6 (2013) 157.
[4] N. Bao, L. Shen, T. Takata, K. Domen, Chem. Mater. 20 (2008) 110.
[5] H. Yu, S.X. Ouyang, S.C. Yan, Z.S. Li, T. Yu, Z.G. Zou, J. Mater. Chem. 21 (2011) 11347.
[6] Z.J. Han, F. Qiu, R. Eisenberg, P.L. Holland, T.D. Krauss, Science 338 (2012) 1321.
[7] T.M. McCormick, B.D. Calitree, A. Orchard, N.D. Kraut, F.V. Bright, M.R. Detty, R. Eisenberg, J. Am. Chem. Soc. 132 (2010) 15480.
[8] S.X. Min, G.X. Lu, Int. J. Hydrogen Energy 38 (2013) 2106.
[9] K. Heussner, K. Peuntinger, N. Rockstroh, L.C. Nye, I. Ivanovic-Burmazovic, S. Rau, C. Streb, Chem. Commun. 47 (2011) 6852.
[10] Y.J. Sun, J.W. Sun, J.R. Long, P.D. Yang, C. Chang, J. Chem. Sci. 4 (2013) 118.
[11] N. Bao, L. Shen, T. Takata, Chem. Mater. 20 (2008) 110.
[12] L. Amirav, A.P. Alivisatos, J. Phys. Chem. Lett. 1 (2010) 1051.
[13] K.A. Brown, S. Dayal, X. Ai, G. Rumbles, P.W. King, J. Am. Chem. Soc. 132 (2010) 9672.
[14] J.S. Luo, L. Ma, T.C. He, C.F. Ng, S.J. Wang, H.D. Sun, H.J. Fan, J. Phys. Chem. C 116 (2012) 11956.
[15] L. Etgar, T. Moehl, S. Gabriel, S.G. Hickey, A. Eychmuller, M. Gratzel, ACS Nano 6 (2012) 3092.
[16] P.V. Kamat, J. Phys. Chem. C 112 (2008) 18737.
[17] M. Misra, S. Banerjee, S.K. Mohapatra, P.P. Das, Chem. Mater. 20 (2008) 6784.
[18] P.V. Kamat, A. Kongkanand, K. Tvrdy, K. Takechi, M. Kuno, J. Am. Chem. Soc. 130 (2008) 4007.
[19] Y.Y. Bu, Z.Y. Chen, W.B. Li, J.Q. Yu, ACS Appl. Mater. Interfaces 5 (2013) 5097.
[20] W.Q. Cui, L. Liu, S.S. Ma, Y.H. Liang, Z.S. Zhang, Catal. Today 207 (2013) 44.
[21] L.J. Liu, L. Lv, G.Q. Xu, Y. Wang, K. Xie, J. Solid State Chem. 208 (2013) 27.
[22] Y. Xie, G. Ail, S.H. Yoo, S.O. Cho, ACS Appl. Mater. Interfaces 2 (2010) 2910.
[23] C.X. Li, L.J. Han, R.J. Liu, H.H. Li, S.J. Zhang, G.J. Zhang, J. Mater. Chem. 22 (2012) 23815.
[24] Y. Liu, Y.X. Yu, W.D. Zhang, J. Phys. Chem. C 117 (2013) 12949.
[25] S.X. Ouyang, J.H. Ye, J. Am. Chem. Soc. 133 (2011) 7757.
[26] Q. Li, H. Meng, P. Zhou, Y.Q. Zheng, J. Wang, J.G. Yu, J.R. Gong, ACS Catal. 3 (2013) 82.
[27] K.H. Reddy, S. Martha, K.M. Parida, Inorg. Chem. 52 (2013) 6390.
[28] P. Saini, M. Arora, G. Gupta, B.K. Gupta, V.N. Singh, V. Choudary, Nanoscale 5 (2013) 4330.
[29] J.G. Yu, Y.F. Yu, B. Cheng, RSC Adv. 2 (2012) 11829.
[30] F. Wang, W.G. Wang, X.J. Wang, H.Y. Wang, C.H. Tung, L.Z. Wu, Angew. Chem. Int. Ed. 50 (2011) 3193.
[31] B.F. Disalle, S. Bernhard, J. Am. Chem. Soc. 133 (2011) 11819.
[32] T. Ohno, L. Bai, T. Hisatomi, K. Maeda, K. Domen, J. Am. Chem. Soc. 134 (2012) 8254.
[33] H.J. Yan, J.H. Yang, G.J. Ma, G.P. Wu, X. Zong, Z.B. Lei, J.Y. Shi, C. Li, J. Catal. 266 (2009) 165.